Variations of Surface Ozone at Ieodo Ocean Research Station in the East China Sea and influence of Asian Outflows

J. Han[1], B. Shin[1,2], M. Lee[1*], G. Hwang[1], J. Kim[1], J. Shim[3], G. Lee[4], C. Shim[5]

[1] Department of Earth & Environmental Sciences, Korea University, Seoul, South Korea

[2] Asian Dust Research Division, National Institute of Meteorological Research, Jeju, South Korea

[3] Coastal Disaster Research Center, Korea Institute of Ocean Science & Technology, Ansan, South Korea

[4]Department of Environmental Science, Hankuk University of Foreign Studies, Yongin, South Korea

[5]Korea Environment Institute, Sejong, South Korea

Submitted to Atmospheric Chemistry and Physics

April 2015

Correspondence to: M. Lee (meehye@korea.ac.kr)

Abstract

Ieodo Ocean Research Station (IORS), a research tower (~40 m a.s.l.) for atmospheric and oceanographic observations, is located in the East China Sea (32.07°N, 125.10°E). The IORS is almost equidistant from South Korea, China, and Japan and, therefore, it is an ideal place to observe Asian outflows without local emission effects. The seasonal variation of ozone was distinct, with a minimum in August (37 ppbv) and two peaks in April and October (62 ppbv), and was largely affected by seasonal wind pattern over East Asia. At IORS, six types of air masses were distinguished with different levels of O_3 concentrations by the cluster analysis of backward trajectories. Marine air masses from the Pacific Ocean represent a relatively clean background air with a lowest ozone level of 32 ppbv, which was most frequently observed in summer (July ~ August). In spring (March~April) and winter (December ~ February), the influence of Chinese outflows was dominant with higher ozone concentrations of 62 ppbv and 49 ppbv, respectively. This study confirms that the influence of Chinese outflows was the main factor determining O_3 levels at IORS, of which extent was dependent on meteorological state, particularly at a long-term scale.

1. Introduction

Ozone (O_3) and its photochemical derivative, OH, are primary oxidants and key players determining oxidation capacity within the troposphere (e.g., Berchet et al., 2013; Seinfeld and Pandis, 2006). A short-lived greenhouse gas, O_3 also affects climate change and air quality (e.g., Berchet et al., 2013; Brasseur et al., 1999; IPCC 2013; Jacobson, 2012). Exposure to high O_3 levels is known to increase human mortality rates (Bell and Dominici, 2008; Chang et al., 2010), reduce agricultural yields, and damage natural ecosystems (e.g., Bell et al., 2011; Karnosky et al., 2007; Schaub et al., 2005; Wang and Mauzerall, 2004). Tropospheric O_3 is primarily transported from the stratosphere upon tropopause folding and produced by *in situ* photochemical reactions involving carbon monoxide (CO) and hydrocarbons in the presence of nitrogen oxides (NO_x) (Brasseur et al., 1999). Ozone is also lost by photochemical reactions and deposition to the Earth's surface. As a result, the lifetime of O_3 ranges from about a week in summer to several months in winter, which permits O_3, along with other pollutants, to be transported over long distances. In previous studies, ozone levels were observed to be enhanced episodically in polluted air masses from continental outflow in remote regions of the North Atlantic and North Pacific Oceans (e.g., Fischer et al., 2011; Lin et al., 2012; Parrish et al., 2009; Zhang et al., 2008).

Particularly, East Asia has experienced a rapid development in economy and industry, from which emissions of O_3 precursors such as NO_x and VOCs have gradually increased (Huang et al., 2013; Monks et al., 2009; Zhao et al., 2013) and the emission of O_3 and its precursors in East Asia is expected to increase further in the near future (Zhao et al., 2013; Ohara et al., 2007). As a result, the study region became a hot spot for high O_3 and intensive measurements have been performed there to chart O_3 and the effects it has in conjunction with climate change. Over the North Pacific Ocean, ozone has been measured on remote islands (Kato et al., 2001; Parrish et al., 2012; Tanimoto et al., 2009; Wada et al., 2011), from ships (Ridder et

al., 2012;Watanabe et al., 2005) and by aircraft (Dupont et al., 2012; Kotchenruther et al., 2001; Walker et al., 2010; Zhang et al., 2008).

The impact of continental outflow upon the background O_3 is substantial in Northeast Asia (Akimoto et al., 1996; Kondo et al., 2008; Tanimoto et al., 2008; Wada et al., 2011; Yamaji et al., 2006). This impact has similarly been detected near the western U.S (Fischer et al., 2011; Lin et al., 2012; Parrish et al., 2009). Walker et al. (2010) estimated that Asian anthropogenic outflow and lightning-derived NO_x emissions contributed at least 7.2 ppbv and 3.5 ppbv to O_3 concentration, respectively, in the North Pacific Ocean and western North America. In addition, Zhang et al. (2008) assessed that O_3 in western North America was increased by Asian outflow 5-7 ppbv during spring 2006. The results of these studies indicate O_3 concentrations in the North Pacific-rim are regularly affected by Asian outflow. Therefore, it is critical to understand the impact of continental outflows from East Asia on O_3 and oxidizing power over the North Pacific Ocean. Since IORS is located in the East China Sea (32.07°N, 125.10°E) (Fig. 1) and almost equidistant from nearby South Korea, China, and Japan, it is an ideal place to observe Asian outflows without local effects (Hwang et al., 2008; Shin et al., 2007). In this study, we present long-term measurements of O_3 at IORS, located in the boundary zone between the Yellow and East China Sea. Then, we describe their characteristic variations and evaluate the continental influence on the regional background concentrations of O_3.

2. Methodology

Ieodo Ocean Research Station is an unmanned research tower (~40 m a.s.l.) for atmospheric and oceanographic observations. It was built on rock 36 m below sea level by the Korea Institute of Ocean Science and Technology (KIOST) in 2003 (Moon et al., 2010; Shim et al., 2004). O_3 has been measured at IORS since June 2003. In addition, meteorological

parameters have been monitored, which include air pressure, air temperature, relative humidity, wind speed and direction, and visibility. O_3 was measured by an UV photometric analyzer (49C, Thermo Inc., U.S.A.) using the absorption of UV radiation at 253.7 nm by O_3 molecules. The analyzer was installed in a dry lab of the main deck, which is 29 m above sea level. Ambient air was pulled underneath the main deck through a 7 m PFA tubing (6 mm-OD). The detection limit of the instrument was 1.0 ppbv. Calibration was done about once every two months with an internal ozonator. In addition, the ozone analyzer was inter-compared with an identical instrument, which was calibrated against the Primary Standard. The two instruments were run side-by-side using a common inlet. The correlation coefficient of the two measurements was 0.99 in the range between 10 and 90 ppbv and ambient measurements were scaled using the relationship between the two.

The data logger stored 10-min averages. There were power failures and system malfunction at IORS when it was hit by typhoon several times. Thus, raw data were first filtered manually and then the measurements bigger and smaller than 2σ (standard deviation) of the average for 10 neighboring values were eliminated. This method is widely used to remove local effects for long-term period measurement (Cvitaš et al., 2004). Statistical analysis was conducted using R (v.3.0.1) (R Core Team, 2014).

Backward trajectories arriving at 100 and 1500 m a.s.l. were calculated for 40 h every 00, 06, 12, and 24 UTC (03, 09, 18, and 21 local time) using the NOAA Air Resources Laboratory (ARL) Hybrid Single-Particle Lagrangian Integrated Trajectory (HYSPLIT) model (version 4) (Draxler and Rolph, 2003, http://www.arl.noaa.gov/ready/hysplit4.html) with NCEP Final Analyses (FNL) six-hourly archived data. Isentropic trajectory was selected as it was believed to reflect a more realistic vertical motion for an adiabatic atmosphere. Forty hours were selected because it was long enough to capture regional transport patterns in the

114 northwestern Pacific and short enough to keep trajectory errors. The results for 100 and 1500
115 m showed no meaningful differences and so the following discussion will be based on 1500 m.
116
117 **3. Ozone variations**
118 The mean concentration of 10 min O_3 measurements was 52 ppbv with a maximum of 128
119 ppbv. The variation of monthly means is presented for eight years, from June 2003 to
120 December 2010 (Fig. 2), during which O_3 increased ~2.8% $year^{-1}$ until 2009 and slightly
121 decreased afterwards. The long-term trend of O_3 at IORS is consistent with recent findings of
122 slowdown in the increase of O_3 concentrations observed in Japanese background stations at
123 Mt. Happo and others (Parrish et al., 2012). This hemispheric baseline likely affects O_3
124 distributions at IORS. Additionally, the vertical column density of tropospheric NO_2 was
125 reported to be decreased over East Asia in 2009, as observed by satellites GOME-2 and
126 SCIAMACHY (Itahashi et al., 2014). In the same context, emissions of NO_x sharply
127 increased in East Asia after 2000 mostly from China, but then slowed down in 2009
128 (Tanimoto et al., 2009; Zhao et al., 2013). Gu et al. (2013) pointed out that the stagnation of
129 NO_x emissions in 2009 were associated with an economic recession in China.
130 The O_3 concentrations of IORS were compared with those of other remote sites in East
131 Asia and the North Pacific for the same period: Gosan in Korea (National Institute of
132 Environmental Research) and Ryori, Yonagunijima, and Minamitorishima in Japan (World
133 Data Centre for Greenhouse Gases (WDCGG), http://ds.data.jma.go.jp/gmd/wdcgg/) (Fig. 1).
134 The diurnal and seasonal variations of eight-year averaged O_3 are presented here in Fig. 3.
135 The averaged O_3 concentrations of IORS, Gosan, Ryori, Yonagunijima, and Minamitorishima
136 were 52, 39, 40, 39, and 27 ppbv, respectively. In these remote sites, the level of averaged O_3
137 concentrations decreased with increased distance from China. At IORS, O_3 mixing ratios
138 show the minimum at 9 a.m. and reached to the broad maximum at 5 p.m. The daytime build-

139 up of O_3 was 5 ppbv, which was much smaller than that in urban areas, but implied in-situ
140 photochemical production for O_3 in the marine boundary layer of the remote site (Fig. 3a).
141 While diurnal patterns of O_3 concentration stayed unchanged through seasons, their
142 background concentrations were clearly different with being the highest in spring and the
143 lowest in summer monsoon season. The daytime build-up of O_3 at Gosan in southern island of
144 Korea and Ryori, located at the northeasterly edge of Japan, were 8 ppbv and 6 ppbv,
145 respectively, significantly greater than 2 ppbv at Yonagunijima (Fig. 3b). Among the five sites,
146 O_3 concentration was reduced in the afternoon only at Minamitorishima, implying O_3
147 destruction. Considering O_3 loss is generally observed under low NOx conditions in the
148 remote marine boundary layer (MBL) (Ayers et al. 1996), these variations indicate that IORS
149 including other remote sites in East Asia were influenced by continental outflows. In the study
150 region, the high concentration of O_3 was reported to be attributed to transport of ozone or its
151 precursors mainly from China (Tanimoto et al., 2008).

152 At IORS, the monthly averaged O_3 concentrations were the highest in April and October
153 (62 ppbv) and lowest in August (37 ppbv) (Fig. 3c). The O_3 concentrations remained high
154 during March ~ May, resulting in a broad spring peak which was in contrast to a sharp fall
155 peak. This is in accordance with a typical pattern that has been observed in other remote sites
156 over Northeast Asia during the past decades (Chan et al., 2002; Jaffe et al., 1996; Kanaya et
157 al., 2015; Kondo et al., 2008; Oltmans and Levy II, 1994; Tanimoto et al., 2005; Tanimoto et
158 al., 2009; Watanabe et al., 2005; Weiss-Penzias et al., 2004). In particular, the second peak of
159 O_3 was the most noticeable at IORS along with Gosan in October, of which tendency was
160 observed in previous studies (Kanaya et al., 2015; Tanimoto et al. 2005). It is also noteworthy
161 that outlier levels were the highest and the maximum concentration (128 ppbv) was observed
162 in July (Fig. 4a). In summer, the study region is under influence of Asian monsoon system
163 which brings moist air from the Pacific Ocean. Meteorological parameters including relative

164 humidity, wind speed, and visibility indicate a clear shift in air mass from pre-monsoon to
165 monsoon season (Fig. 4b). At IORS, O_3 concentration was noticeably decreased during
166 summer, even though temperature was high. Likewise, the O_3 level of Gosan was reduced
167 down to the minimum in summer, when the levels of precursors were the lowest with heavy
168 rainfall. To examine seasonal characteristics of O_3 distributions, all measured species were
169 divided into five seasons: March–April, May–June (pre-monsoon period), July–August,
170 September–November, and December–February. The seasonal wind patterns are presented in
171 Figure 5.

172 All O_3 measurements showed bimodal distribution, with a little shoulder on the larger peak
173 (Fig. 6a). In seasonal distributions, the smaller peak (25 ppbv) was the main mode of summer
174 monsoon season. As shown in Figure 5, southerly winds were dominant during July–August
175 (82%) under the influence of North Pacific High. This pattern reveals that the decrease in O_3
176 was associated with the aged marine air masses brought by the North Pacific High or tropical
177 cyclones (Fig. 5c). In addition to aged air masses, precipitation had scavenged O_3 precursors,
178 possibly leading to lowered O_3 concentrations (Hou et al., 2015). It was also observed that O_3
179 was decreased in Beijing and Shanghai during the summer monsoon season (Safieddine et al.,
180 2013). In May–June, the mode concentration was the highest at 65 ppbv with the least
181 frequency (Fig. 6c). It is a transition period from continental air mass to oceanic air mass and,
182 as a result, the stagnant conditions which had developed under high temperature without
183 prevailing wind (Fig. 5b), led to elevated O_3 concentrations. The mode concentration was the
184 second highest (59 ppbv) in spring, which is characterized by the most effective transport of
185 Chinese outflow by the passage of frontal system (Hou et al., 2014; Kondo et al., 2008; Lim et
186 al., 2012). The mode frequency was the greatest in winter, which was due to prevailing
187 northerly winds accounting for ~87% of that period. The main mode of winter and fall, and
188 the second mode of summer monsoon season displayed similar concentrations, which

189 comprised the primary mode of O_3 distributions observed at IORS. O_3 levels are known to
190 exhibit lower variability at remote sites and rural areas (McKendry et al., 2014; Oltmans and
191 Levy II, 1994). However, the results of this study challenge those of previous studies. O_3
192 concentrations of IORS were highly dependent on air masses, upon which anthropogenic
193 influence was in a wide variation. This finding emphasizes the significant role of continental
194 outflows in determining O_3 concentrations in the Northeast Asian region.
195

196 **4. Source signatures of O_3**

197 **4.1. Cluster analysis of air mass trajectories**

198

199 Trajectories were divided into several groups using an agglomerative and hierarchical
200 clustering algorithm with an average linkage function. Average linkage minimizes the within-
201 cluster variance while maximizing between-cluster variance and has been identified as an
202 effective method for categorizing different synoptic situations (Kalkstein et al., 1987). Within
203 a cluster, the root mean square deviation (RMSD) of each trajectory from the cluster center
204 was quantified and then summed to give the total root mean square deviation (TRMSD) (Cape
205 et al., 2000). As a result, six trajectories were identified. The cluster analysis was performed
206 using the Openair package in R (Carslaw and Ropkins, 2012, 2014). The distance matrix was
207 calculated by the Euclidean distance.

208 The averaged backward trajectories of each cluster are presented in a map (Fig. 7). Among
209 the six clusters, W was the most dominant (23.0 %), followed by NW1 (19.9 %), N (17.9 %),
210 SE (16.6 %), SW (13.4 %), and NW2 (9.2 %). The average O_3 concentration was the highest
211 for N (60 ppbv) and lowest for SE (40 ppbv). For the four clusters of continental air masses,
212 the mean O_3 concentrations were similar to the mean (52 ppbv) of the entire measurement set.

In contrast, the marine air masses of SE and SW were characterized by low O_3 concentrations, particularly during summer (32 ppbv).

4.2. Source signature by CWT (Concentration Weighted Trajectory) analysis

The CWT (Concentration Weighted Trajectory) method was employed to figure out the potential source of O_3 observed at IORS. The concentration of O_3 for each grid-cell was calculated using the following equation (Carslaw, 2013):

$$\ln(\bar{C}_{ij}) = \frac{1}{\sum_{l=1}^{N} \tau_{ijl}} \sum_{l=1}^{N} ln(c_l)\tau_{ijl} \qquad (1)$$

where, i and j indicate the indices of grid, N shows the entire number of backward trajectories, l represents the index of trajectory, c_l signifies the concentration of O_3 observed upon arrival of trajectory l, and τ_{ijl} is the residence time of trajectory l in the grid-cell (i, j) (Carslaw, 2013; Cheng et al., 2013). In Fig. 8, the average O_3 concentrations were presented over each grid-cell. The O_3 concentration was notably higher for NW1 when air mass passed through the Beijing region. The trajectory of NW2 was similar to that of NW1 except for vertical movement, which is typical for air masses laden with Asian dusts (e.g., Kang et al., 2013).

Because the trajectory length is inversely proportional to the residence time of air in a grid-cell, the clusters N and W represent stagnant conditions, which was favorable for O_3 to build up. These two trajectories were constantly observed through the year with relatively less seasonal variation at IORS (Fig. 9b). Although the air masses of SW and SE originated from the Pacific Ocean, they were likely to pick urban emissions up when passing through the Southeastern China and South Japan, respectively. The result of CWT analysis confirms that the outflows from nearby lands were the source of O_3 observed at IORS, of which the Chinese influence was the most dominant.

4.3. Influence of Asian continental outflows

For all clusters, the monthly variations of O_3 concentrations were compared (Fig. 9a). In general, six clusters were similar in their annual pattern of O_3, with higher concentrations in spring and fall and lower concentrations in summer. In contrast, for NW1, which passes through the Beijing metro area, O_3 concentrations stayed high over 60 ppbv during July–August without considerable decrease (Fig. 9a). Although the summer concentrations in SE were low, below 30 ppbv, in spring and fall the O_3 concentration were high and comparable to those of NW1.

The influence of Chinese outflows, represented by NW1, NW2, and W, was highest in winter, with a maximum occurrence (86%) in December. The study region is under influence of Asian monsoon and is characterized by winds southerly in summer and northerly in winter. The occurrence of maritime air, SE and SW, was the most frequent in summer monsoon season. The westerlies prevalent in this region are coupled with the steady occurrence of W through the year, implying a constant influence of Chinese outflows. The cluster N was commonly observed before and after summer monsoon season, during which a stagnant condition often developed under the influence of migratory anticyclone systems. It used to park over the Yellow Sea, accumulating pollutants from nearby lands including China, Japan as well as Korea. In fact, the high concentrations of O_3 turned out to be associated with air trajectories from Chinese coastal regions. The model results of Zhao et al. (2009) also showed that the high concentration of O_3 can be expanded under a high pressure system in East Asia.

The annual variation of each cluster was examined (Fig. 10a). As the O_3 measurement began in June 2003, the measurements of 2003 were not included in this analysis. The yearly O_3 concentrations increased from 49 ppbv in 2004 to 55 ppbv in 2009 and then decreased to 49 ppbv in 2010 (Fig. 2). This pattern was not reflected in NW1 and NW2, for which annual means were the highest in 2004 and lowest in 2010. Marine air masses, including SE and SW,

showed the most visible change during this period. Particularly, their annual frequencies increased in 2010, while those of clusters W, N, NW1 decreased (Fig. 10b). These results imply that marine air masses were likely to play a significant role in decreasing O_3 concentration in 2010. The causes underlying increased occurrence of marine air masses needs to be further investigated. These results suggest that a decrease in O_3 concentrations after 2009 was not only associated with the decrease in NO_x emission from China, but also a change in meteorological state in the study region.

Considering that Chinese influence is implicit in N and SW, Chinese emission was the predominant factor determining the concentrations of O_3 at IORS. The impact of Korean and Japanese emissions were incorporated in N and SE, apparent in spring and fall, respectively.

5. Conclusion

Surface O_3 concentrations were determined at Ieodo Ocean Research Station (IORS) in the East China Sea (32.07°N, 125.10°E) from June 2003 to December 2010. The IORS is a 40 m research tower roughly equidistant from Korean, Chinese, and Japanese shores. The average concentration of O_3 for the entire period was of 52 ± 16 ppbv. It is higher than those of remote sites in the Northeast Asia and implies the steady influence of continental outflows. Particularly, the seasonal differences were prominent, with two peaks in April and October (62 ppbv) and a minimum in August (37 ppbv), which are greatly dependent on synoptic scale circulation of the atmosphere which, except for summer, expedites effective transport of Asian outflows into the Northwest Pacific region. The diurnal variation of O_3 showed a broad maximum in late afternoon, resulting in 5 ppbv of daytime build-up.

The cluster analysis of backward trajectories identified the six air masses affecting O_3 concentrations at IORS. Among the six, four types of air masses originated from Asian continents, carrying their outflows (NW1, NW2, W, and N) and the other two were aged

marine air from the Pacific Ocean (SE, SW). The O_3 concentration of these continental and marine air masses was the maximum (62 ppbv) in spring and minimum (32 ppbv) in summer, respectively. Particularly, the three clusters of NW1, NW2, and W, coming directly from mainland China, comprised 53% of all air masses which arrived at IORS, their contribution increasing up to ~86% in winter. The clusters N and W were the most frequent under stagnant condition before and after summer monsoon. In summer, the occurrence of marine air reached the maximum (~74%). These results confirm that Chinese emissions were the dominant source of O_3 observed at IORS.

The annual O_3 concentrations increased until 2009, and then slightly decreased in 2010, which is in good accordance with NO_x observed in East Asia, where a slowdown of NO_x emission occurred in 2009 as a result of economic recession in China. In addition, the cluster analysis of air masses highlighted the increased contribution of marine air masses also played a role in decreasing mean concentration of O_3 in 2010.

Acknowledgements

This study was sponsored by the Ministry of Oceans and Fisheries through the Korea Institute of Ocean Science and Technology (KIOST). We thank the people who contributed to establish IORS and who participated in field measurements. A part of this study was done as the master's thesis of Beomcheol Shin.

References

Akimoto, H., Mukai, H., Nishikawa, M., Murano, K., Hatakeyama, S., Liu, C.-M., Buhr, M., Hsu, K. J., Jaffe, D. A., Zhang, L., Honrath, R., Merrill, J. T., and Newell, R. E.: Long-range transport of ozone in the East Asian Pacific rim region, J. Geophys. Res. Atmos., 101, 1999-2010, doi:10.1029/95JD00025, 1996.

Ayers, G. P., Penkett, S. A., Gillett, R. W., Bandy, B., Galbally, I. E., Meyer, C. P., Elsworth, C. M., Bentley, S. T., and Forgan, B. W.: The annual cycle of peroxides and ozone in marine air at Cape Grim, Tasmania, J. Atmos. Chem., 23, 221-252, doi:10.1007/BF00055155, 1996.

Bell, J. N. B., Power, S. A., Jarraud, N., Agrawal, M., and Davies, C.: The effects of air pollution on urban ecosystems and agriculture, Int. J. Sustain. Dev. World Ecol., 18, 226-235, doi:10.1080/13504509.2011.570803, 2011.

Bell, M. L. and Dominici, F.: Effect modification by community characteristics on the short-term effects of ozone exposure and mortality in 98 US communities, Amer. J. Epidemiol., 167, 986-997, doi:10.1093/aje/kwm396, 2008.

Berchet, A., Paris, J. D., Ancellet, G., Law, K. S., Stohl, A., Nédélec, P., Arshinov, M. Y., Belan, B. D., and Ciais, P.: Tropospheric ozone over Siberia in spring 2010: Remote influences and stratospheric intrusion, Tellus B, 65, 19688, doi:10.3402/tellusb.v65i0.19688, 2013.

Brasseur, G. P., Orlando, J. J., and Tyndall, G. S.: Atmospheric chemistry and global change, Oxford University Press, New York, 654 pp., 1999.

Cape, J. N., Methven, J., and Hudson, L. E.: The use of trajectory cluster analysis to interpret trace gas measurements at Mace Head, Ireland, Atmos. Environ., 34, 3651-3663, doi:10.1016/S1352-2310(00)00098-4, 2000.

Carslaw, D. C.: The openair manual - open-source tools for analyzing air pollution data. Manual for version 0.8-0, King's College London, 2013.

Carslaw, D. C. and Ropkins, K.: openair - an R package for air quality data analysis. Environmental Modeling & Software, 27-28, 52-61, 2012.

Carslaw, D. C. and Ropkins, K.: openair: Open-source tools for the analysis of air pollution data. R package version 0.9-2, King's College London, 2014.

335 Chan, C. Y., Chan, L. Y., Lam, K. S., Li, Y. S., Harris, J. M., and Oltmans, S. J.: Effects of
336 Asian air pollution transport and photochemistry on carbon monoxide variability and ozone
337 production in subtropical coastal South China, J. Geophys. Res., 107, 4746,
338 doi:10.1029/2002JD002131, 2002.

339 Chang, H. H., Zhou, J., and Fuentes, M.: Impact of Climate Change on Ambient Ozone Level
340 and Mortality in Southeastern United States, Int. J. Environ. Res. Public Heal., 7, 2866-2880,
341 doi:10.3390/ijerph7072866, 2010.

342 Cheng, I., Zhang, L., Blanchard, P., Dalziel, J., and Tordon, R.: Concentration-weighted
343 trajectory approach to identifying potential sources of speciated atmospheric mercury at an
344 urban coastal site in Nova Scotia, Canada, Atmos. Chem. Phys., 13, 6031-6048,
345 doi:10.5194/acp-13-6031-2013, 2013.

346 Cvitaš, T., Furger, M., Girgzdiene, R., Haszpra, L., Kezele, N., Klasinc, L., Planinšek, A.,
347 Pompe, M., Prevot, A. S. H., Scheel, H. E., and Schuepbach, E.: Spectral analysis of boundary
348 layer ozone data from the EUROTRAC TOR network, J. Geophys. Res., 109, D02302,
349 doi:10.1029/2003JD003727, 2004.

350 Draxler, R. R., and Rolph, G. D.: HYSPLIT (HYbrid Single-Particle Lagrangian Integrated
351 Trajectory) Model access via NOAA ARL READY website, NOAA Air Resource Lab.,
352 Silver Spring, Md., Available at: http://www.arl.noaa.gov/ready/hysplit4.html (last access: 11
353 June 2015), 2003.

354 Dupont, R., Pierce, B., Worden, J., Hair, J., Fenn, M., Hamer, P., Natarajan, M., Schaack, T.,
355 Lenzen, A., Apel, E., Dibb, J., Diskin, G., Huey, G., Weinheimer, A., Kondo, Y., and Knapp,
356 D.: Attribution and evolution of ozone from Asian wild fires using satellite and aircraft
357 measurements during the ARCTAS campaign, Atmos. Chem. Phys., 12, 169-188,
358 doi:10.5194/acp-12-169-2012,2012.

359 Fischer, E. V., Jaffe, D. A., and Weatherhead, E. C.: Free tropospheric peroxyacetyl nitrate
360 (PAN) and ozone at Mount Bachelor: potential causes of variability and timescale for trend
361 detection, Atmos. Chem. Phys., 11, 5641-5654, doi:10.5194/acp-11-5641-2011, 2011.

362 Gu, D., Wang, Y., Smeltzer, C., and Liu, Z.: Reduction in NOx Emission Trends over China:
363 Regional and Seasonal Variations, Environ. Sci. Technol., 47, 12912-12919,
364 doi:10.1021/es401727e, 2013.

Hou, X., Zhu, B., Kang, H., and Gao, J.: Analysis of seasonal ozone budget and spring ozone latitudinal gradient variation in the boundary layer of the Asia-Pacific region, Atmos. Environ., 94, 734-741, doi:10.1016/j.atmosenv.2014.06.006, 2014.

Hou, X., Zhu, B., Fei, D., and Wang, D.: The impacts of summer monsoons on the ozone budget of the atmospheric boundary layer of the Asia-Pacific region, Sci. Total Environ., 502, 641-649, doi:10.1016/j.scitotenv.2014.09.075, 2015.

Huang, J., Zhou, C., Lee, X., Bao, Y., Zhao, X., Fung, J., Richter, A., Liu, X., and Zheng, Y.: The effects of rapid urbanization on the levels in tropospheric nitrogen dioxide and ozone over East China, Atmos. Environ., 77, 558-567, 2013.

Hwang, G., Lee, M., Shin, B., Lee, G., Lee, J., and Shim, J.: Mass Concentration and Ionic Composition of $PM_{2.5}$ Observed at Ieodo Ocean Research Station, Korean J. of Atmos. Environ., 24, 501-511, 2008 (in Korean with English abstract).

IPCC: Climate Change 2013: The Physical Science Basis, Intergovernmental Panel on Climate Change, edited by: Stocker, T. F., Qin, D., Plattner, G.-K., Tignor, M., Allen, S. K., Boschung, J., Nauels, A., Xia, Y., Bex, V., and Midgley, P. M., Cambridge University Press, Cambridge, 1535 pp., 2013.

Itahashi, S., Uno, I., Irie, H., Kurokawa, J. I., and Ohara, T.: Regional modeling of tropospheric NO_2 vertical column density over East Asia during the period 2000–2010: comparison with multisatellite observations, Atmos. Chem. Phys., 14, 3623-3635, doi:10.5194/acp-14-3623-2014, 2014.

Jacobson, M. Z.: Air Pollution and Global Warming: History, Science, and Solutions, 2nd Edn., Cambridge University Press, Cambridge, 406 pp., 2012.

Jaffe, D. A., Honrath, R. E., Zhang, L., Akimoto, H., Shimizu, A., Mukai, H., Murano, K., Hatakeyama, S., and Merrill, J.: Measurements of NO, NOy , CO and O_3 and estimation of the ozone production rate at Oki Island, Japan, during PEM-West, J. Geophys. Res.-Atmos., 101, 2037-2048, doi:10.1029/95JD01699, 1996.

Kalkstein, L. S., Tan, G., and Skindlov, J. A.: An Evaluation of Three Clustering Procedures for Use in Synoptic Climatological Classification, J. Clim. Appl. Meteorol., 26, 717-730, doi:10.1175/1520-0450(1987)026<0717:AEOTCP>2.0.CO;2, 1987.

394 Kang, E., Han, J., Lee, M., Lee, G., and Kim, J. C.: Chemical characteristics of size-resolved
395 aerosols from Asian dust and haze episode in Seoul Metropolitan City, Atmos. Res., 127, 34-
396 46, doi:10.1016/j.atmosres.2013.02.002, 2013.

397 Kanaya, Y., Tanimoto, H., Yokouchi, Y., Taketani, F., Komazaki, Y., Irie, H., Takashima, H.,
398 Pan, X., Nozoe, S., and Inomata, S.: Diagnosis of Photochemical Ozone Production Rates and
399 Limiting Factors in Continental Outflow Air Masses Reaching Fukue Island, Japan: Ozone-
400 Control Implications, Aerosol Air Qual. Res., doi: 10.4209/aaqr.2015.04.0220, 2015.

401 Karnosky, D. F., Skelly, J. M., Percy, K. E., and Chappelka, A. H.: Perspectives regarding 50
402 years of research on effects of tropospheric ozone air pollution on US forests, Environ. Pollut.,
403 147, 489-506, doi:10.1016/j.envpol.2006.08.043, 2007.

404 Kato, S., Pochanart, P., and Kajii, Y.: Measurements of ozone and nonmethane hydrocarbons
405 at Chichi-jima island, a remote island in the western Pacific: long-range transport of polluted
406 air from the Pacific rim region, Atmos. Environ., 35, 6021-6029, doi:10.1016/S1352-
407 2310(01)00453-8, 2001.

408 Kondo, Y., Hudman, R. C., Nakamura, K., Koike, M., Chen, G., Miyazaki, Y., Takegawa, N.,
409 Blake, D. R., Simpson, I. J., Ko, M., Kita, K., Shirai, T., and Kawakami, S.: Mechanisms that
410 influence the formation of high-ozone regions in the boundary layer downwind of the Asian
411 continent in winter and spring, J. Geophys. Res., 113, D15304, doi:10.1029/2007JD008978,
412 2008.

413 Kotchenruther, R. A., Jaffe, D. A., Beine, H. J., Anderson, T. L., Bottenheim, J. W., Harris, J.
414 M., Blake, D. R., and Schmitt, R.: Observations of ozone and related species in the Northeast
415 Pacific during the PHOBEA campaigns: 2. Airborne observations, J. Geophys. Res., 106,
416 7463-7483, doi:10.1029/2000JD900425, 2001.

417 Lim, S., Lee, M., Lee, G., Kim, S., Yoon, S., and Kang, K.: Ionic and carbonaceous
418 compositions of PM_{10}, $PM_{2.5}$ and $PM_{1.0}$ at Gosan ABC Superstation and their ratios as source
419 signature, Atmos. Chem. Phys., 12, 2007-2024, doi:10.5194/acp-12-2007-2012, 2012.

420 Lin, M., Fiore, A. M., Horowitz, L. W., Cooper, O. R., Naik, V., Holloway, J., Johnson, B. J.,
421 Middlebrook, A. M., Oltmans, S. J., Pollack, I. B., Ryerson, T. B., Warner, J. X., Wiedinmyer,
422 C., Wilson, J., and Wyman, B.: Transport of Asian ozone pollution into surface air over the
423 western United States in spring, J. Geophys. Res., 117, D00V07, doi:10.1029/2011jd016961,
424 2012.

McKendry, I., Christensen, E., Schiller, C., Vingarzan, R., Macdonald, A. M., and Li, Y.: Low Ozone Episodes at Amphitrite Point Marine Boundary Layer Observatory, British Columbia, Canada, Atmos. Ocean, 52, 271-280, doi:10.1080/07055900.2014.910164, 2014.

Monks, P. S., Granier, C., Fuzzi, S., Stohl, A., Williams, M. L., Akimoto, H., Amann, M., Baklanov, A., Baltensperger, U., Bey, I., Blake, N., Blake, R. S., Carslaw, K., Cooper, O. R., Dentener, F., Fowler, D., Fragkou, E., Frost, G. J., Generoso, S., Ginoux, P., Grewe, V., Guenther, A., Hansson, H. C., Henne, S., Hjorth, J., Hofzumahaus, A., Huntrieser, H., Isaksen, I. S. A., Jenkin, M. E., Kaiser, J., Kanakidou, M., Klimont, Z., Kulmala, M., Laj, P., Lawrence, M. G., Lee, J. D., Liousse, C., Maione, M., McFiggans, G., Metzger, A., Mieville, A., Moussiopoulos, N., Orlando, J. J., O'Dowd, C. D., Palmer, P. I., Parrish, D. D., Petzold, A., Platt, U., Pöschl, U., Prévôt, A. S. H., Reeves, C. E., Reimann, S., Rudich, Y., Sellegri, K., Steinbrecher, R., Simpson, D., ten Brink, H., Theloke, J., van der Werf, G. R., Vautard, R., Vestreng, V., Vlachokostas, C., and von Glasow, R.: Atmospheric composition change – global and regional air quality, Atmos. Environ., 43, 5268-5350, doi:10.1016/j.atmosenv.2009.08.021, 2009.

Moon, I.-J., Shim, J.-S., Lee, D. Y., Lee, J. H., Min, I.-K., and Lim, K. C.: Typhoon Researches Using the Ieodo Ocean Research Station : Part1. Importance and Present Status of Typhoon Observation, Atmosphere (Korean Meteorological Society), 20, 247-260, 2010 (in Korean with English abstract).

Ohara, T., Akimoto, H., Kurokawa, J., Horii, N., Yamaji, K., Yan, X., and Hayasaka, T.: An Asian emission inventory of anthropogenic emission sources for the period 1980–2020, Atmos. Chem. Phys., 7, 4419-4444, doi:10.5194/acp-7-4419-2007, 2007.

Oltmans, S. J., and Levy II, H.: Surface ozone measurements from a global network, Atmos. Environ., 28, 9-24, doi:10.1016/1352-2310(94)90019-1, 1994.

Parrish, D. D., Millet, D. B., and Goldstein, A. H.: Increasing ozone in marine boundary layer inflow at the West coasts of North America and Europe, Atmos. Chem. Phys., 9, 1303-1323, doi:10.5194/acp-9-1303-2009, 2009.

Parrish, D. D., Law, K. S., Staehelin, J., Derwent, R., Cooper, O. R., Tanimoto, H., Volz-Thomas, A., Gilge, S., Scheel, H. E., Steinbacher, M., and Chan, E.: Long-term changes in lower tropospheric baseline ozone concentrations at northern mid-latitudes, Atmos. Chem. Phys., 12, 11485-11504, doi:10.5194/acp-12-11485-2012, 2012.

R Core Team, R.: A language and environment for statistical computing. R Foundation for Statistical Computing, Vienna, Austria. available at: http://www.R-project.org/ (last access: 11 June 2015), 2014.

Ridder, T., Gerbig, C., Notholt, J., Rex, M., Schrems, O., Warneke, T., and Zhang, L.: Ship-borne FTIR measurements of CO and O3 in the Western Pacific from 43° N to 35° S: an evaluation of the sources, Atmos. Chem. Phys., 12, 815-828, doi:10.5194/acp-12-815-2012, 2012.

Safieddine, S., Clerbaux, C., George, M., Hadji-Lazaro, J., Hurtmans, D., Coheur, P. F., Wespes, C., Loyola, D., Valks, P., and Hao, N.: Tropospheric ozone and nitrogen dioxide measurements in urban and rural regions as seen by IASI and GOME-2, J. Geophys. Res., 118, 10555-10566, 2013.

Schaub, M., Skelly, J. M., Zhang, J. W., Ferdinand, J. A., Savage, J. E., Stevenson, R. E., Davis, D. D., and Steiner, K. C.: Physiological and foliar symptom response in the crowns of Prunus serotina, Fraxinus americana and Acer rubrum canopy trees to ambient ozone under forest conditions, Environ. Pollut., 133, 553-567, doi:10.1016/j.envpol. 2004.06.012, 2005.

Seinfeld, J. H., and Pandis, S. N.: Atmospheric Chemistry and Physics: From Air Pollution to Climate Change, 2nd Edn., John Wiley and Sons, New York, 2006.

Shim, J. H., Chun, I. S., and Min, I. K.: Construction of Ieodo Ocean Research Station and its operation, The Proceedings of the 14th International Offshore and Polar Engineering Conference, 23–28 May 2004, Toulon, France, 140, 13–11, 2004.

Shin, B., Lee, M., Lee, J., and Shim, J. S.: Seasonal and Diurnal Variations of Surface Ozone at Ieodo in the East China Sea, Korean J. of Atmos. Environ., 23, 631-639, 2007 (in Korean with English abstract).

Tang, G., Li, X., Wang, Y., Xin, J., and Ren, X.: Surface ozone trend details and interpretations in Beijing, 2001–2006, Atmos. Chem. Phys., 9, 8813-8823, doi:10.5194/acp-9-8813-2009, 2009.

Tanimoto, H., Sawa, Y., Matsueda, H., Uno, I., Ohara, T., Yamaji, K., Kurokawa, J.-i., and Yonemura, S.: Significant latitudinal gradient in the surface ozone spring maximum over East Asia, Geophys. Res. Lett., 32, L21805, doi:10.1029/2005GL023514, 2005.

485 Tanimoto, H., Sawa, Y., Yonemura, S., Yumimoto, K., Matsueda, H., Uno, I., Hayasaka, T.,
486 Mukai, H., Tohjima, Y., Tsuboi, K., and Zhang, L.: Diagnosing recent CO emissions and
487 ozone evolution in East Asia using coordinated surface observations, adjoint inverse modeling,
488 and MOPITT satellite data, Atmos. Chem. Phys., 8, 3867-3880, doi:10.5194/acp-8-3867-2008,
489 2008.

490 Tanimoto, H., Ohara, T., and Uno, I.: Asian anthropogenic emissions and decadal trends in
491 springtime tropospheric ozone over Japan: 1998–2007, Geophys. Res. Lett., 36, L23802,
492 doi:10.1029/2009GL041382, 2009.

493 Wada, A., Matsueda, H., Sawa, Y., Tsuboi, K., and Okubo, S.: Seasonal variation of
494 enhancement ratios of trace gases observed over 10 years in the western North Pacific, Atmos.
495 Environ., 45, 2129-2137, 2011.

496 Walker, T. W., Martin, R. V., van Donkelaar, A., Leaitch, W. R., MacDonald, A. M., Anlauf,
497 K. G., Cohen, R. C., Bertram, T. H., Huey, L. G., Avery, M. A., Weinheimer, A. J., Flocke, F.
498 M., Tarasick, D. W., Thompson, A. M., Streets, D. G., and Liu, X.: Trans-Pacific transport of
499 reactive nitrogen and ozone to Canada during spring, Atmos. Chem. Phys., 10, 8353-8372,
500 doi:10.5194/acp-10-8353-2010, 2010.

501 Wang, S. X., Zhao, B., Cai, S. Y., Klimont, Z., Nielsen, C., McElroy, M. B., Morikawa, T.,
502 Woo, J. H., Kim, Y., Fu, X., Xu, J. Y., Hao, J. M. and He, K. B.: Emission trends and
503 mitigation options for air pollutants in East Asia, Atmos. Chem. Phys., 14, 6751-6603,
504 doi:10.5194/acp-14-6571-2014, 2014.

505 Wang, X. and Mauzerall, D. L.: Characterizing distributions of surface ozone and its impact
506 on grain production in China, Japan and South Korea: 1990 and 2020, Atmos. Environ., 38,
507 4383-4402, doi:10.1016/j.atmosenv.2004.03.067, 2004.

508 Watanabe, K., Nojiri, Y., and Kariya, S.: Measurements of ozone concentrations on a
509 commercial vessel in the marine boundary layer over the northern North Pacific Ocean, J.
510 Geophys. Res., 110, D11310, doi:10.1029/2004JD005514, 2005.

511 Weiss-Penzias, P., Jaffe, D. A., Jaeglé, L., and Liang, Q.: Influence of long-range-transported
512 pollution on the annual and diurnal cycles of carbon monoxide and ozone at Cheeka Peak
513 Observatory, J. Geophys. Res., 109, D23S14, doi:10.1029/2004JD004505, 2004.

514 Yamaji, K., Ohara, T., Uno, I., Tanimoto, H., Kurokawa, J.-i., and Akimoto, H.: Analysis of
515 the seasonal variation of ozone in the boundary layer in East Asia using the Community

516 Multi-scale Air Quality model: What controls surface ozone levels over Japan?, Atmos.
517 Environ., 40, 1856-1868, doi:10.1016/j.atmosenv.2005.10.067, 2006.

518 Zhang, L., Jacob, D. J., Boersma, K. F., Jaffe, D. A., Olson, J. R., Bowman, K. W., Worden, J.
519 R., Thompson, A. M., Avery, M. A., Cohen, R. C., Dibb, J. E., Flock, F. M., Fuelberg, H. E.,
520 Huey, L. G., McMillan, W. W., Singh, H. B., and Weinheimer, A. J.: Transpacific transport of
521 ozone pollution and the effect of recent Asian emission increases on air quality in North
522 America: An integrated analysis using satellite, aircraft, ozonesonde, and surface observations,
523 Atmos. Chem. Phys., 8, 6117-6136, doi:10.5194/acp-8-6117-2008, 2008.

524 Zhao, B., Wang, S. X., Liu, H., Xu, J. Y., Fu, K., Klimont, Z., Hao, J. M., He, K. B., Cofala,
525 J., and Amann, M.: NOx emissions in China: historical trends and future perspectives, Atmos.
526 Chem. Phys., 13, 9869-9897, doi:10.5194/acp-13-9869-2013, 2013.

527 Zhao, C., Wang, Y., and Zeng, T.: East China plains: A "basin" of ozone pollution, Environ.
528 Sci. Technol., 43, 1911-1915, 2009.

529 **Figure Captions**

530

531 Figure 1. Geographical locations of (a) Ieodo Ocean Research Station and (b) Gosan, Korea,
532 and (c) Ryori, (d) Yonagunijima, and (e) Minamitorishima, Japan.

533 Figure 2. Monthly mean O_3 concentrations at IORS, from June 2003 to December 2010, with
534 smoothed trend (thick line) and estimated 95% confidence interval (gray shade).

535 Figure 3. Comparison of diurnal and seasonal variations of O_3 concentrations at remote sites
536 in the Northwest Pacific region including IORS, Gosan, Yonagunijima, Ryori, and
537 Minamitorishima. All data were averaged for 8 years (2003–2010) and seasons
538 were divided into spring (May-April), dry summer (May- June), wet summer (July-
539 August), fall (September-November), and winter (December-February). a) diurnal
540 variations of O_3 at IORS in different seasons, b) diurnal variations of O_3 at five sites,
541 and b) monthly variations of O_3 at five sites.

542 Figure 4. a) Monthly variations of O_3 presented with median, interquartile range (IRQ),
543 1.5IQR, and outliers and b) monthly distributions of temperature, relative humidity,
544 wind speed, and visibility at IORS.

545 Figure 5. The left panel for contour maps presenting NCEP/NCAR reanalysis wind speed in
546 color and wind vector at 850 mb in East Asia from 2004 to 2010 and the right panel
547 for windroses measured at IORS during (a) March–April, (b) May–June, (c) July–
548 August, (d) September–November, and (e) December–February.

549 Figure 6. Frequency distributions of 10 min averaged O_3 concentrations at IORS for a) all data,
550 b) spring, c) dry summer, d) wet summer, e) fall, and f) winter with mode
551 concentrations given.

552 Figure 7. Mean trajectories of air masses classified into 6 groups. Air masses of 1500 altitude
553 were traced backward for 40 h.

554 Figure 8. Concentration Weighted Trajectory (CWT) analysis of O_3 concentrations (ppbv).

555 Figure 9. Monthly variations of a) O_3 concentrations of six clusters and b) their monthly
556 frequency.

557 Figure 10. Annual variations of a) O_3 concentrations for six clusters, b) their frequency.

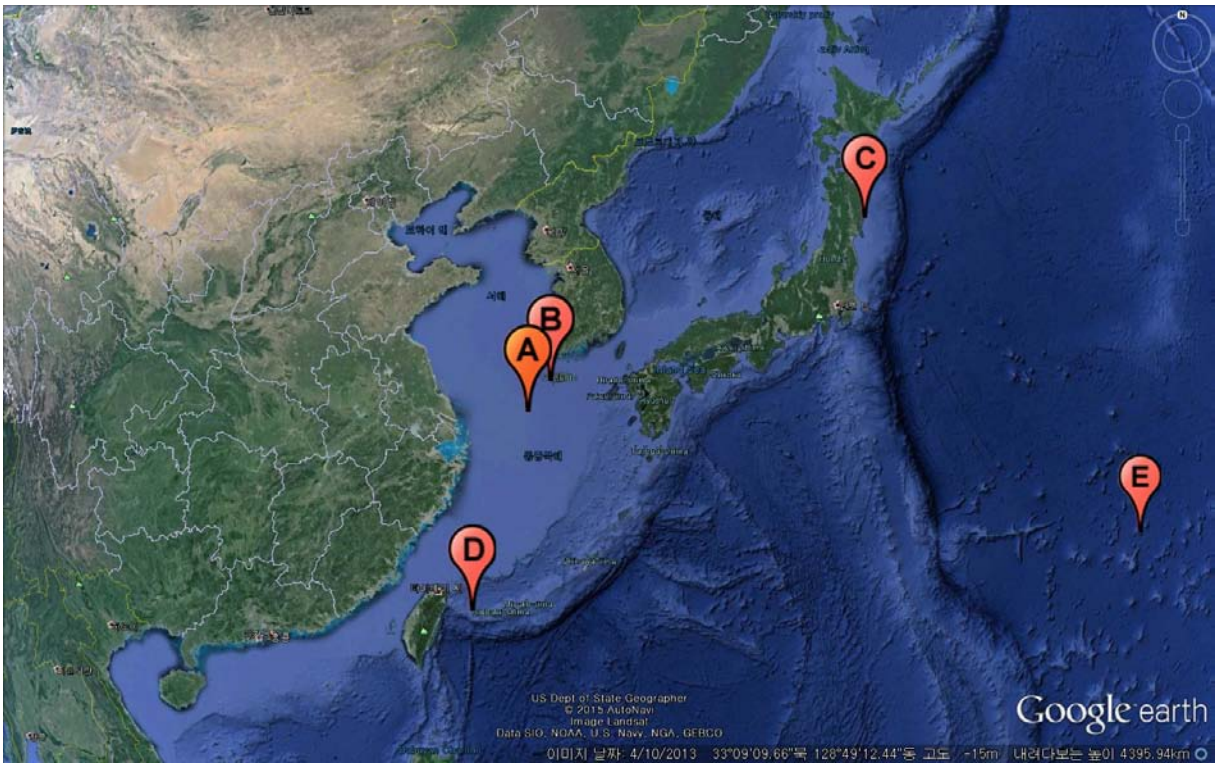

Figure 1. Geographical locations of (a) Ieodo Ocean Research Station and (b) Gosan, Korea, and (c) Ryori, (d) Yonagunijima, and (e) Minamitorishima, Japan.

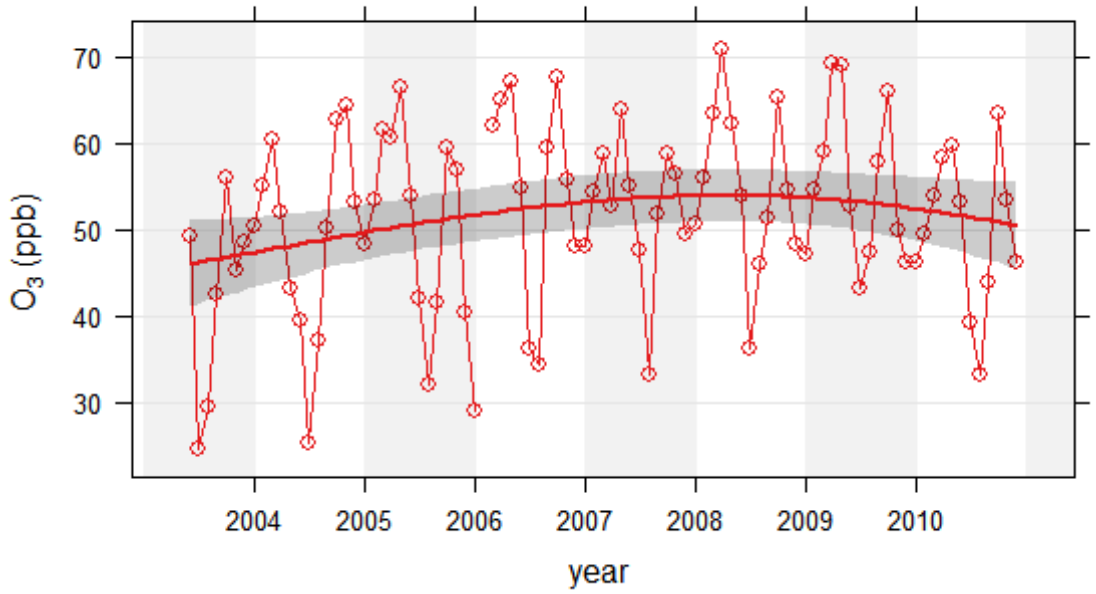

561

562 Figure 2. Monthly mean O_3 concentrations at IORS, from June 2003 to December 2010, with
563 smoothed trend (thick line) and estimated 95% confidence interval (gray shade).

564 a)

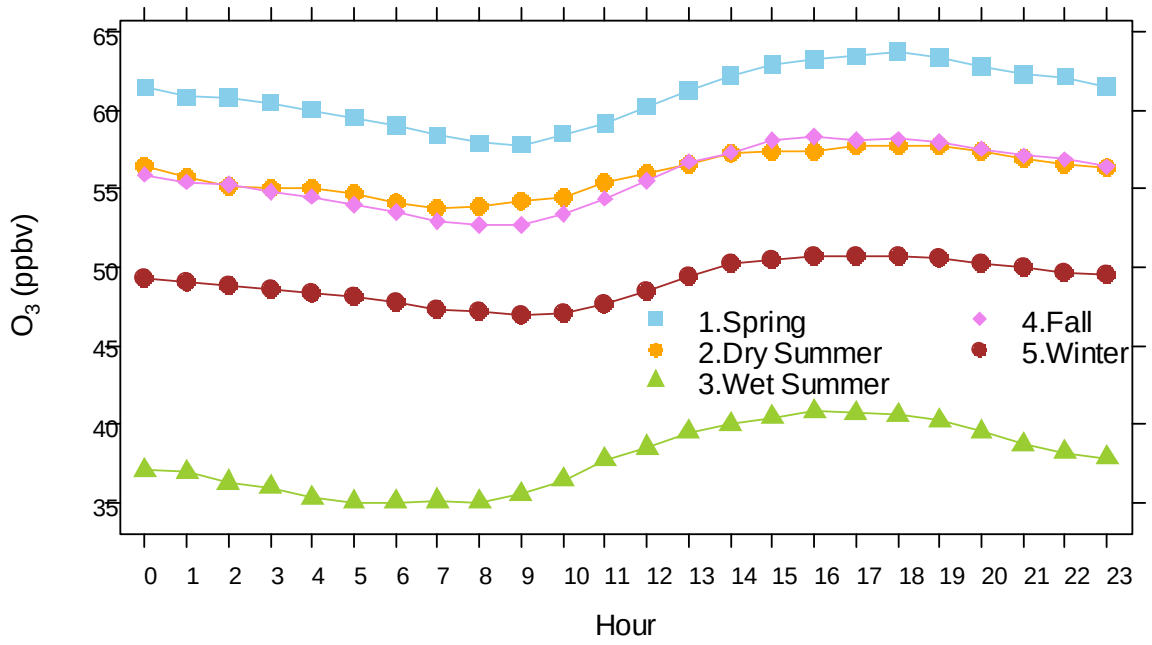

565

566 b)

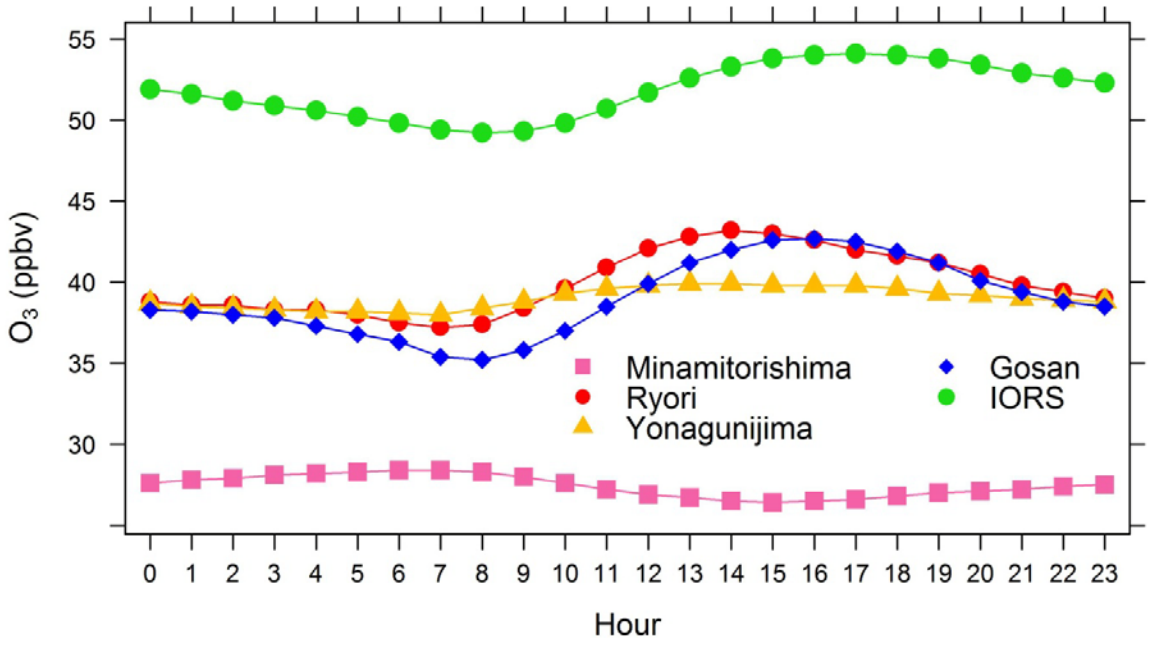

567

568

569 c)

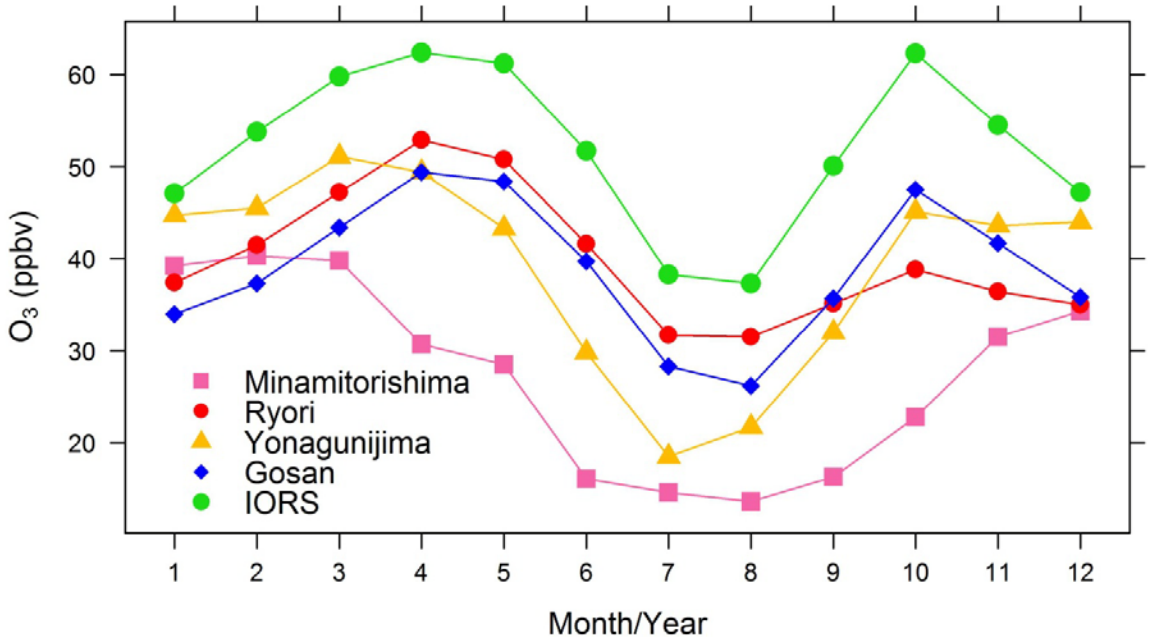

570

571 Figure 3. Comparison of diurnal and seasonal variations of O_3 concentrations at remote sites
572 in the Northwest Pacific region including IORS, Gosan, Yonagunijima, Ryori, and
573 Minamitorishima. All data were averaged for 8 years (2003–2010) and seasons
574 were divided into spring (May-April), dry summer (May- June), wet summer (July-
575 August), fall (September-November), and winter (December-February). a) diurnal
576 variations of O_3 at IORS in different seasons, b) diurnal variations of O_3 at five sites,
577 and c) monthly variations of O_3 at five sites.

578 a)

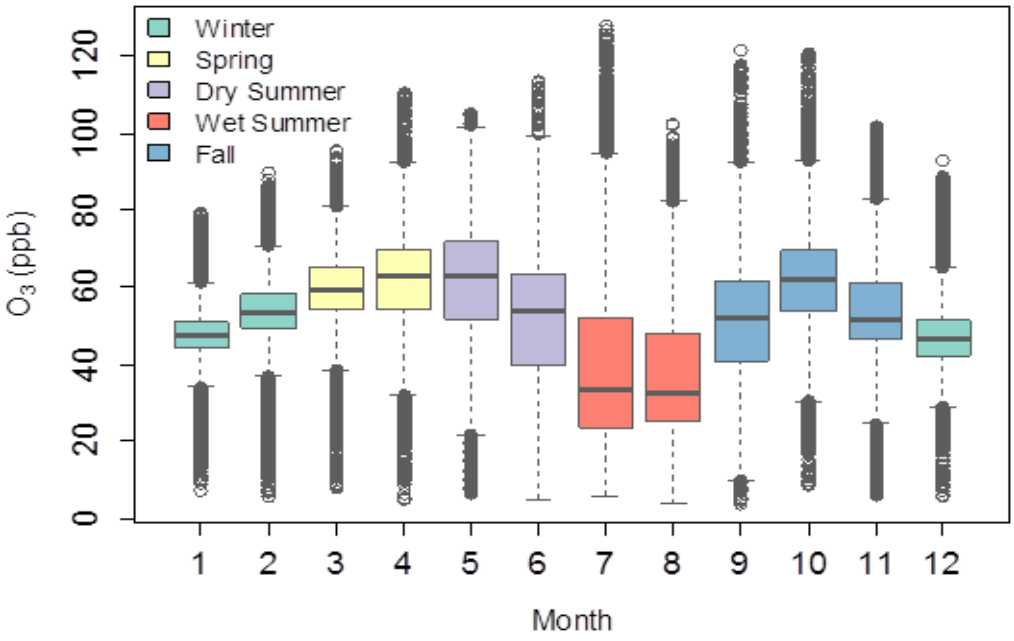

579

580 b)

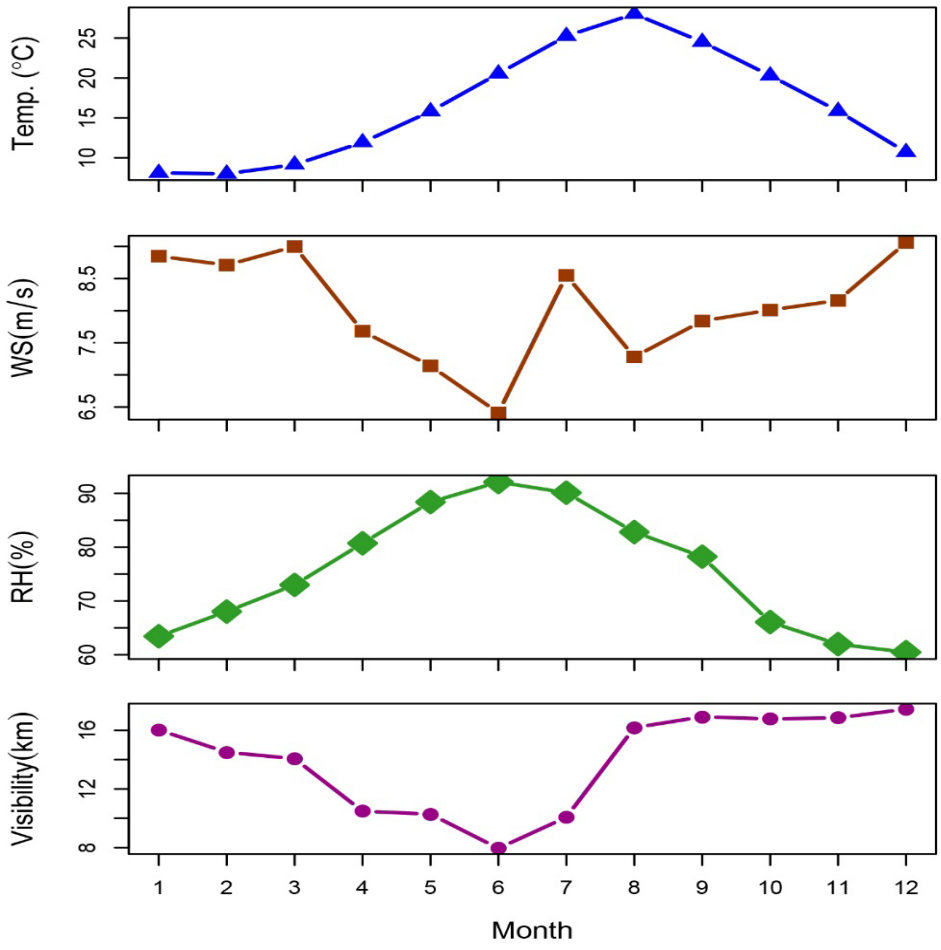

581

582 Figure 4. a) Monthly variations of O_3 presented with median, interquartile range (IQR),
583 1.5IQR, and outliers and b) monthly distributions of temperature, relative humidity,
584 wind speed, and visibility at IORS.

585

586

587 (a)

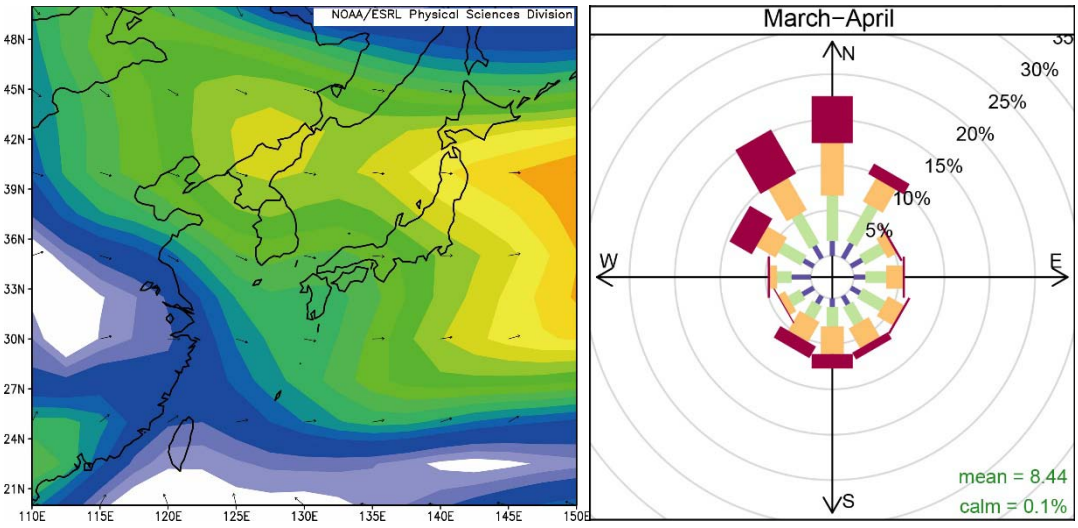

588

589 (b)

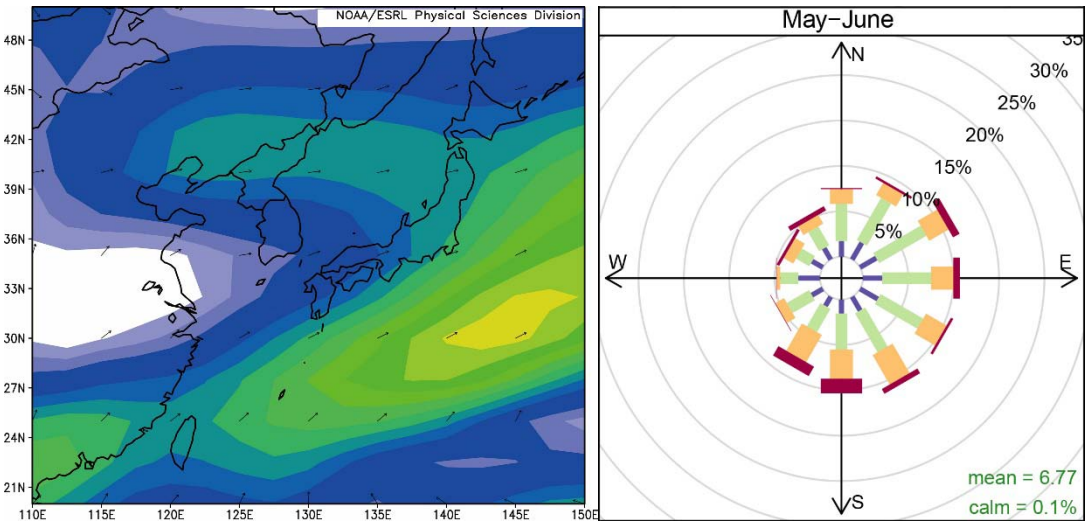

590

591 (c)

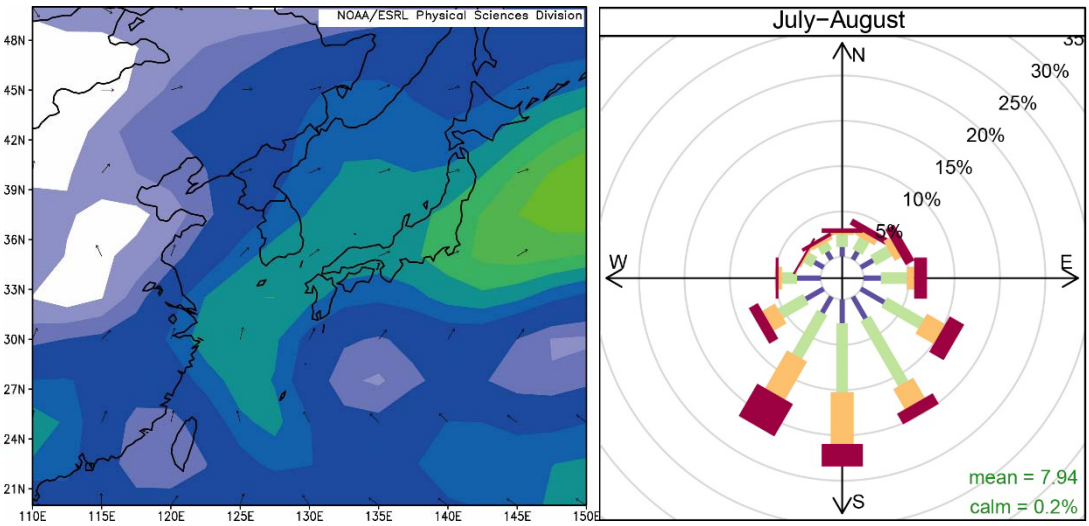

592

(d)

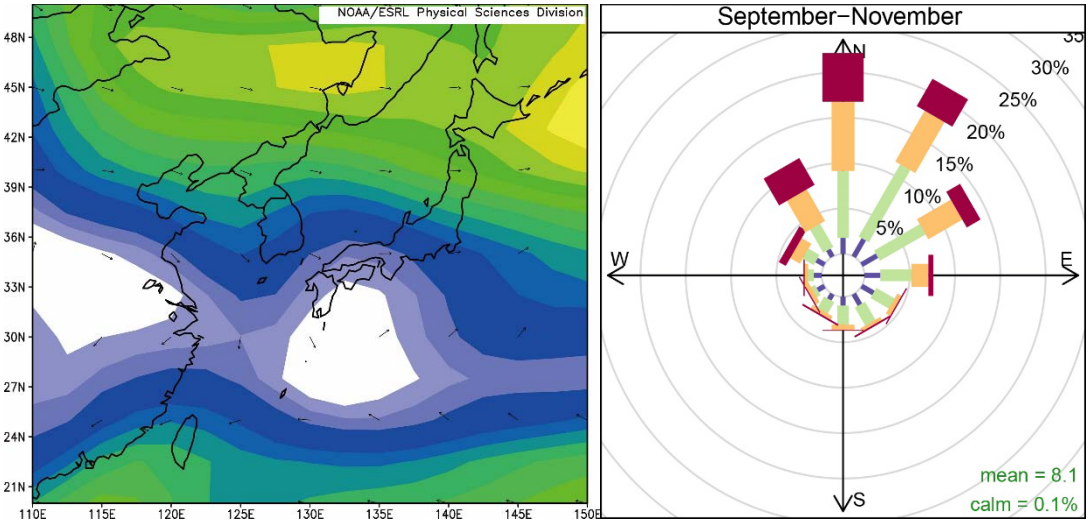

(e)

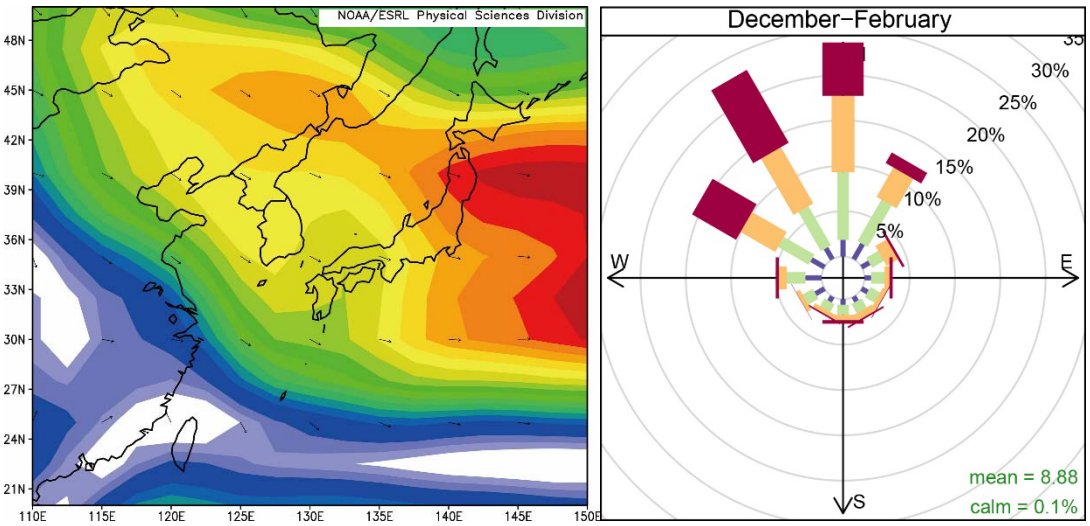

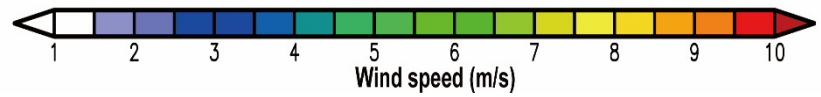

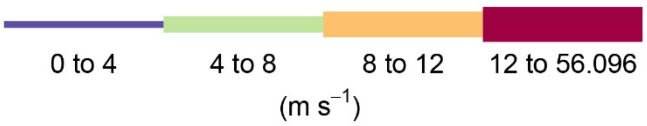

Frequency of counts by wind direction (%)

Figure 5. The left panel for contour maps presenting NCEP/NCAR reanalysis wind speed in color and wind vector at 850 mb in East Asia from 2004 to 2010 and the right panel for windroses measured at IORS during (a) March–April, (b) May–June, (c) July–August, (d) September–November, and (e) December–February.

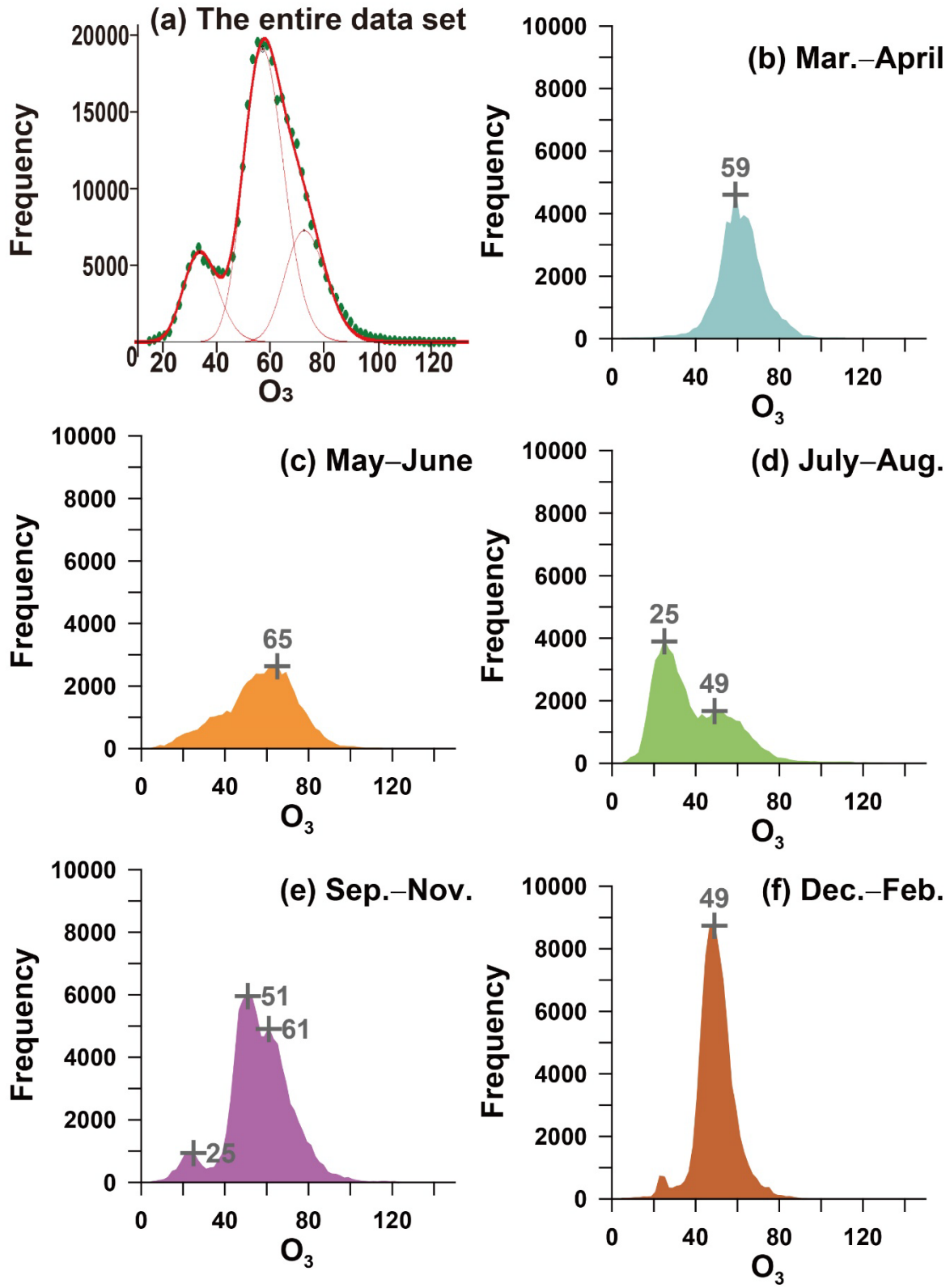

603

604 Figure 6. Frequency distributions of 10 min averaged O_3 concentrations at IORS for a) all data,
605 b) spring, c) dry summer, d) wet summer, e) fall, and f) winter with mode
606 concentrations given.

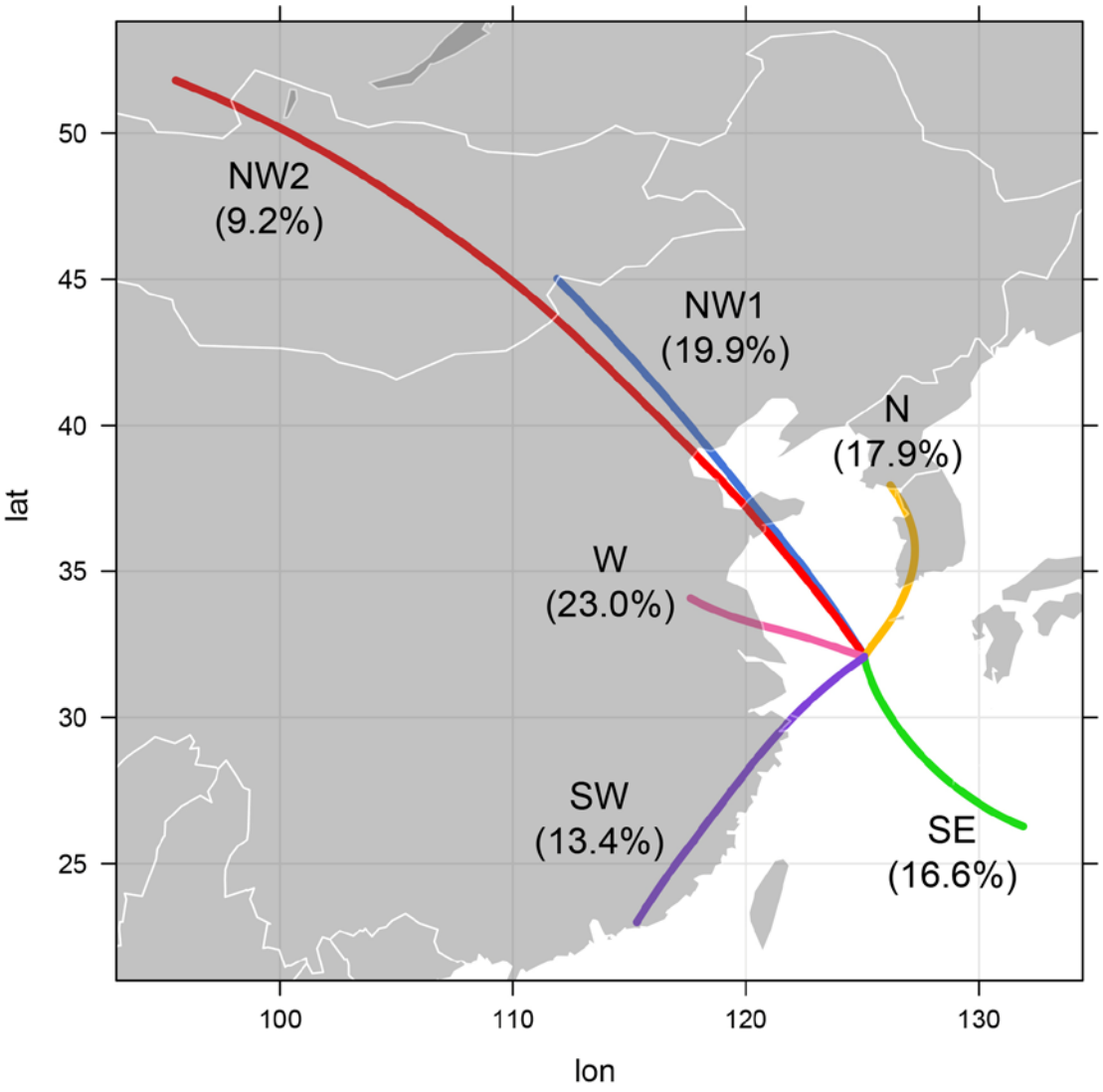

607

608 Figure 7. Mean trajectories of air masses classified into 6 groups. Air masses of 1500 altitude
609 were traced backward for 40 h.

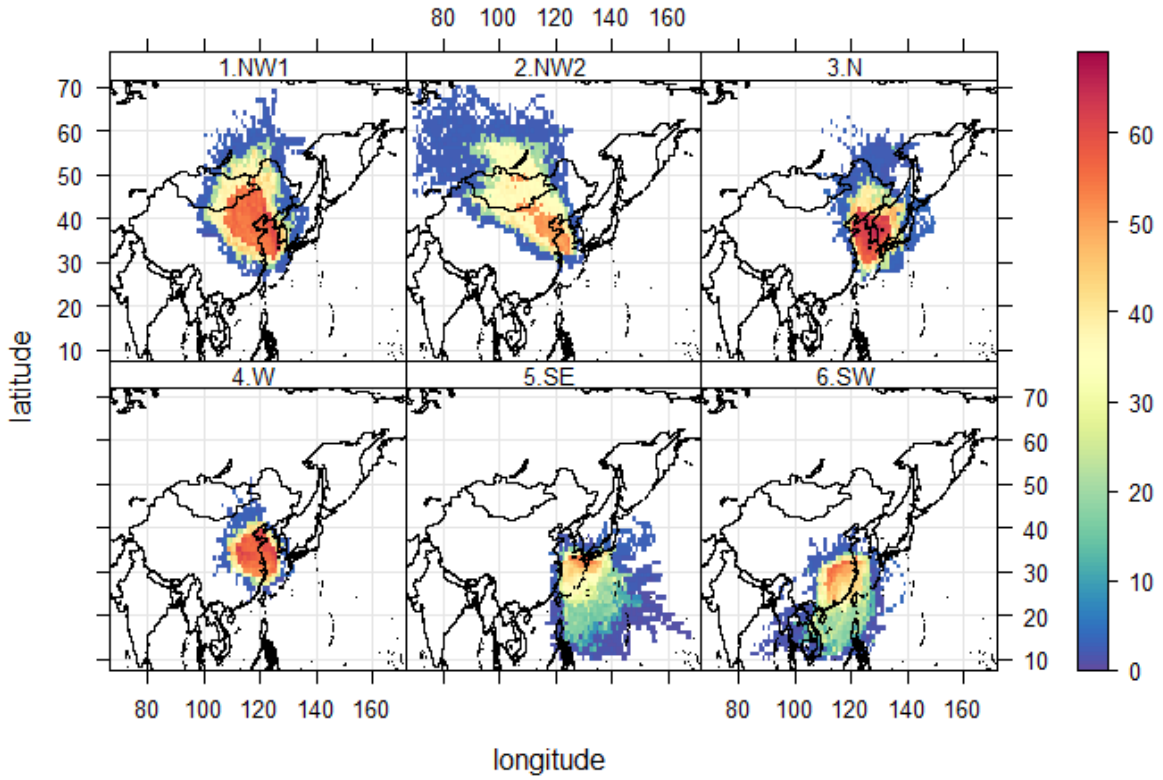

610

611 Figure 8. Concentration Weighted Trajectory (CWT) analysis of O_3 concentrations (ppbv).

612 a)

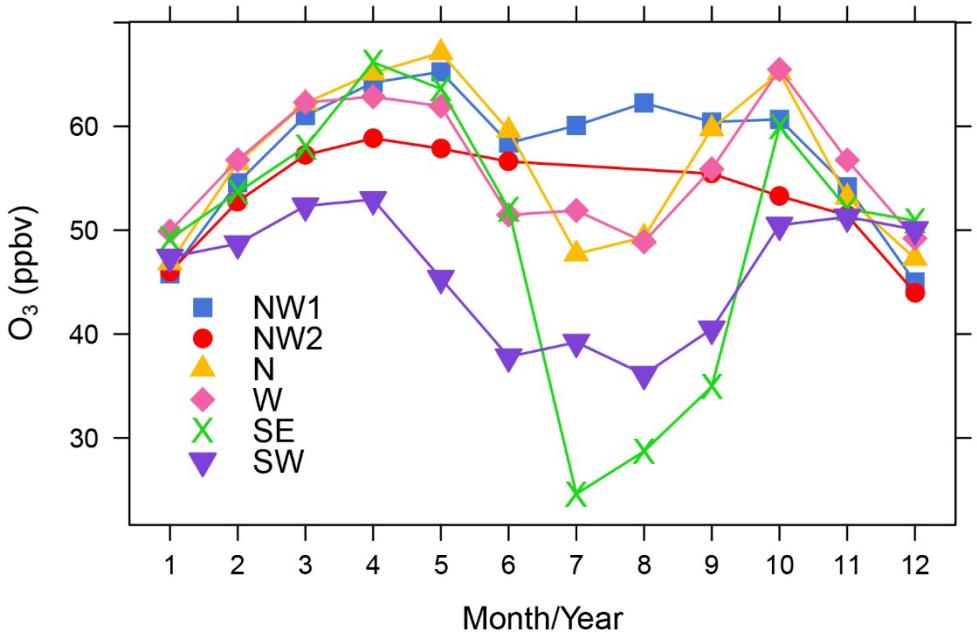

613

614 b)

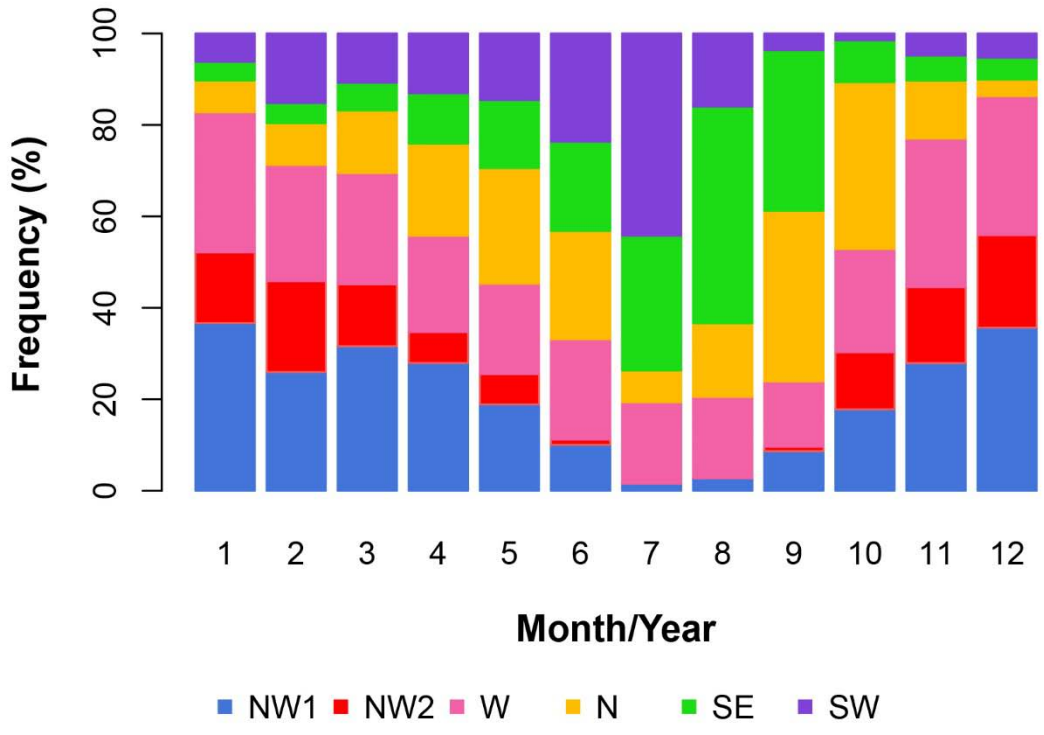

615

616 Figure 9. Monthly variations of a) O_3 concentrations of six clusters and b) their monthly
617 frequency.

618 a)

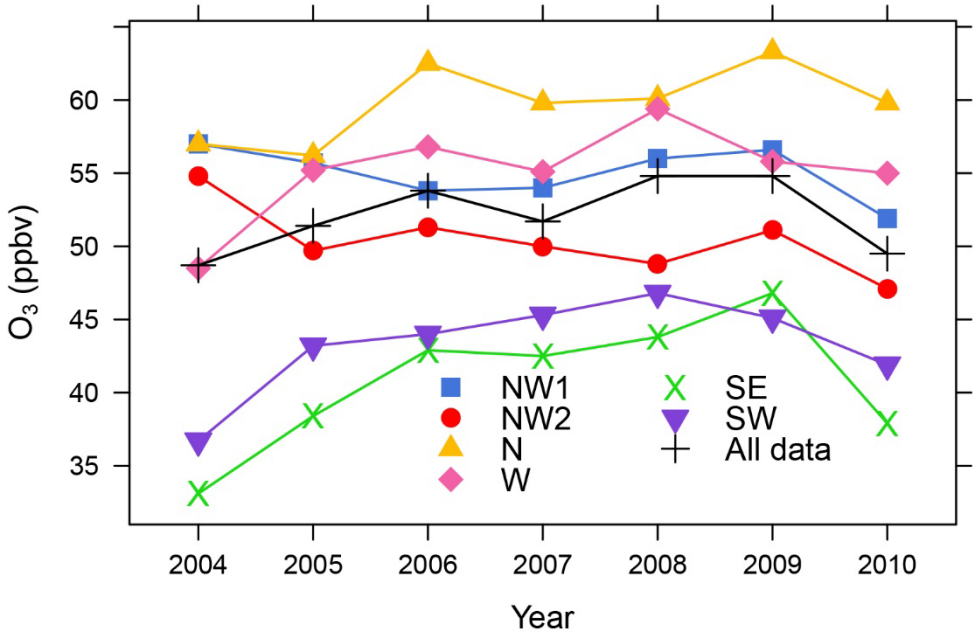

619

620 b)

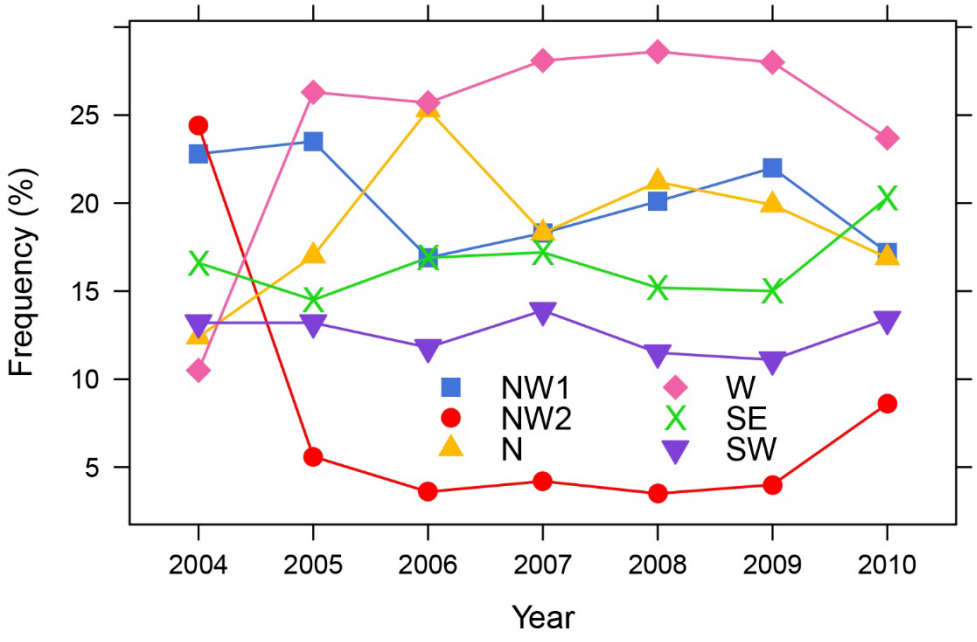

621

622 Figure 10. Annual variations of a) O_3 concentrations for six clusters, b) their frequency.

623